NASA

Technical Memorandum **80307**

(NASA-TM-80307) MAGNETIC FIELD DIRECTIONAL DISCONTINUITIES. 1: MINIMUM VARIANCE ERRORS (NASA) 39 p HC A03/MF A01 CSCL 03B

N79-31116

Unclas
G3/90 36075

Magnetic Field Directional Discontinuities: 1. Minimum Variance Errors

R. P. Lepping and K. W. Behannon

JUNE 1979

National Aeronautics and
Space Administration

Goddard Space Flight Center
Greenbelt, Maryland 20771

MAGNETIC FIELD DIRECTIONAL DISCONTINUITIES:
1. MINIMUM VARIANCE ERRORS

R. P. Lepping and K. W. Behannon
Laboratory for Extraterrestrial Physics
NASA/Goddard Space Flight Center
Greenbelt, Maryland 20771

June 1979

ABSTRACT

An investigation of the errors associated with the minimum variance analysis of directional discontinuity normal components has been performed. This study consisted of both computer simulation of discontinuities with controlled properties and the examination of actual discontinuities (current sheets) observed by the Mariner 10 spacecraft. The simulated discontinuities were created by adding fluctuations, represented by isotropic noise, to exactly known but varying (in a plane) magnetic field components. An empirical expression for the magnitude of the error in an estimated discontinuity normal component, relative to the total field across the discontinuity, was derived, as well as other relevant statistical properties. This formula results from studies of the relation between precisely known values of the error and the minimum variance eigenvalues, rotation angle in the discontinuity plane, and magnitude of the normal component relative to that of the discontinuity plane field component. Use of the empirical relation in the analysis of 644 discontinuities observed by Mariner 10 has provided a more precise but probably conservative estimate of a upper bound on the relative normal component value for tangential discontinuities that can be used to separate rotational from tangential discontinuities in studies using only magnetic field data from a single spacecraft, at least for the interplanetary region of space considered.

INTRODUCTION

Over the past decade various studies concerning the properties of (non-shock front) magnetic field directional discontinuities, or current sheets, have been carried out using only magnetic field data from a single spacecraft (see for example: Burlaga, 1969 and 1971; Turner and Siscoe, 1971; Sonnerup, 1971; Smith, 1973a, b; Siscoe, 1974; and Tsurutani and Smith, 1979). On those occasions when plasma data were available, they were sampled too infrequently to aid in determining the most fine scale characteristics that are amenable to rapidly sampled magnetic field data analysis. However, when available, the use of the associated plasma data is always desirable, especially for determining the discontinuity jump conditions and possibly also for determining if the discontinuity was a propagating or a solely convecting structure. In any case, we will be concerned here with discontinuity analyses that depend only on rapidly sampled magnetic fields measured on a single spacecraft, and, in particular, with the <u>errors</u> associated with estimating various properties, e.g., the errors in the direction of the estimated normal to the discontinuity plane, the estimated angle across the discontinuity in that plane, etc. Also we will restrict our treatment to the errors associated with the use of the so-called minimum variance (MV) analysis developed by Sonnerup and Cahill (1967) which is applied to difference fields; such a field is defined as the difference between the individual field vectors within the discontinuity and the average field across the discontinuity. A similar technique developed by Siscoe et al. (1968), which is applied to the total field vectors in the current sheet, is more properly applicable to a particular subset of directional discontinuities, the tangential discontinuities. The Sonnerup-Cahill method is applicable to both the rotational (RD) and tangential (TD) types (see Burlaga, 1969 for definitions of RD's and TD's, and Burlaga et al., 1977 for a discussion of the relative applicability issue).

Sonnerup (1971) has performed an analysis of the expected error in the magnetic field component perpendicular to the discontinuity plane. The resulting formula gives the normal component error in terms of the average field components in the discontinuity plane and the three eigenvalues obtained from the minimum variance analysis of the field vectors measured within the discontinuity structure. Also included is a term representing a systematic magnetometer zero level error contribution. This present error analysis was motivated by a desire to obtain more physical insight into the errors and limitations associated with use of the minimum variance analysis than is provided by the Sonnerup error formulation. In this study it will be assumed that the input data have been sufficiently corrected for zero level offsets so that explicit incorporation of such instrument-related contributions to the analysis error can be neglected.

Specifically, the error analysis pursued here consists of two major parts: (1) the computer simulation of realistic directional discontinuities with controlled and known properties and the subsequent statistical error study, and (2) the examination of actual Mariner 10 interplanetary magnetic field data from the point of view of error estimations based on information derived from the first part of the study. One of the most important considerations is how well the minimum variance analysis is able to estimate the field component perpendicular to the directional discontinuity (DD) plane, i.e., the normal component, particularly in the presence of various levels of fluctuations in the background field.

By definition a TD has no normal component, and an RD can have any normal component greater than zero but less than the instantaneous magnitude of the total field within the discontinuity (Burlaga, 1969, 1971). The total magnitude change across a TD is unrestricted, but for an RD in an isotropic plasma this quantity is zero. The total magnitude change for an RD in an anisotropic plasma can be nonzero (Ivanov, 1970; Hudson, 1970), and thus, in this one respect, it behaves like a TD. Knowledge of the total magnitude change across a DD is therefore of insufficient help in unambiguously distinguishing between a TD or an RD. In actuality <u>both</u> TD's and RD's in the solar wind, for instance, usually show only slight changes in magnitude across the structure (Burlaga, 1969; Siscoe, 1974) easily accounted for by the extraneous presence of waves or other less easily defined fluctuations - all lumped together as "noise". Hence, we will not depend here on using the total field magnitude jump to distinguish between TD's and RD's, but we will show that such a consideration is of some use via an analysis of Mariner 10 data. We will, however, attempt to use the normal field estimate to make a restricted differentiation. There are types of structures, such as magnetic holes (Turner et al., 1977) and sector boundaries, within which the field magnitude is substantially reduced in addition to a discontinuous change in direction. Possible error in the minimum variance analysis of such structures is not addressed by this present study. However, we shall return briefly to the problem of slight magnitude variations in a later section.

If B_z is the normal field component and B is the total field, ideally when $|B_z|/B$ is zero the DD is a TD, and when $0 < |B_z|/B < 1$, the DD is an RD. One is immediately faced with the obvious dilemma: when $|B_z|/B \gtrsim 0$ for the DD, is it an RD or TD? Using only magnetic field data from a single spacecraft precludes a definitive answer. (Multiple spacecraft and/or plasma data, however, could permit a differentiation based on propagation vs. non-propagation of the DD; see for example Denskat and Burlaga, 1977). All one can logically expect under these restrictions is to estimate for a set of DD's a value of $|B_z|/B$ which is an upper bound on the region of uncertainty, called $(|B_z|/B)_M$; the lower bound is obviously zero. One can then properly attempt to estimate to 95% certainty the value of $(|B_z|/B)$ above which only RD's exist. It may in turn be plausibly argued that the majority of DD's somewhat below the value of $(|B_z|/B)_M$ are probably TD's as Burlaga et al. (1977) did in their study of typical interplanetary DD's at 1 A.U., where the occurrence distribution's appearance aided in identification. But it must be stressed that this sort of TD identification rests on an uncertain foundation. We will be forced to do the same, however, although we have attempted through this error analysis to give our interpretation a more rigorous foundation than the earlier analyses had. More will be said on this point in the discussion of the Mariner 10 data.

THE METHOD OF ANALYSIS: DD SIMULATION

In the DD computer simulation program, an ideal DD is created with strictly known characteristics. Such a DD is shown schematically in Figure 1. Isotropic, unbiased "noise" is added to each magnetic field vector, throughout the transition zone, from a random number generator whose output provides a normally distributed random variable, where inputs to the routine are a fixed zero mean and a variable standard distribution. The noise is also scaled isotropically by the magnitude of the field in the discontinuity plane for all three components. The simulation program uses a fixed angular separtion ($\Delta\omega$) between adjacent discontinuity-plane projected magnetic field vectors; each vector is then computed from:

$$B_{xi} = B_p\,[\cos(\Delta\omega\cdot i) + n_i],$$

$$B_{yi} = B_p\,[\sin(\Delta\omega\cdot i) + n_i],$$

and

$$B_{zi} = B_n + B_p n_i,$$

where B_p is the magnitude of the unperturbed field component in the plane of rotation (i.e., the true discontinuity plane), B_n is the unperturbed normal field component, n_i is the output of the random number generator and $\vec{B}_i = (B_{xi}, B_{yi}, B_{zi})$ is the perturbed field vector at point i. In this fashion K vector are computed ($i = 1,\ldots,K$) where K is selected to give the desired total angle ω in the discontinuity plane. Figure 1 shows only the first (subscript 1) and last (subscript K) vectors of the set. Each set of field vectors generated in this way is subsequently and arbitrarily transformed out of the discontinuity (i.e., "true") coordinate frame, where $B_{zT} = B_n$, and where the unperturbed B_{xT} and B_{yT} are in the true plane of rotation. The transformed set of vectors comprising the simulated DD are then used as inputs to the Sonnerup-Cahill minimum variance (MV) analysis, which then returns the eigenvalues and eigenvectors associated with the MV solution. The eigenvector associated with the minimum eigenvalue is a unit vector whose direction is an <u>estimate</u> of the true z-coordinate direction, and the minimum eigenvalue (λ_3) itself is the variance of the field associated with the estimated direction. Likewise, the maximum and intermediate eigenvalues (λ_1 and λ_2, respectively) are variances of the field along the maximum and intermediate eigenvector directions, which form an orthogonal set with respect to the minimum eigenvector.

For each input value of the standard deviation of the noise distribution (for fixed values of ω, B_p, and B_n) the process of generating a simulated discontinuity and performing the minimum variance analysis is repeated 100 times. This gives distributions of the relevant solution quantities, whose statistics are then computed. For a given set of ideal DD properties, the program loops through an adjustable number of noise levels, creating a full suite of sets from "quiet" to "noisy", usually 10 to 20 sets in all. The process is repeated for another set of ideal DD properties, and so on until a reasonable spectrum of DD's is created. In summary, the three adjustable ideal properties are:

B_p, the magnitude of the field in the discontinuity plane which remains constant as the field rotates through the angle ω;

ω, the angle in the discontinuity plane spanned by the first and last discontinuity plane field vectors;

and B_n, the magnitude of the normal component which has a fixed value throughout the event. (Thus each $B_z \equiv \langle B_{zi} \rangle$ plays the role of an "estimate" of B_n that has been perturbed by the "noise" added to the system.)

The remaining adjustable property is:

σ_B, the standard deviation of a "noise" distribution whose sample, η, the noise factor, enters in the form of $\eta \times B_p$; this term is added to all components isotropically.

Typical values for these quantities have been: 2.5 and 5.6 nT (nT = nanotesla = 10^{-5} Gauss) for B_p; 0 and 5 nT for B_n; 20°, 30°, 45°, 60°, 90°, 120° for ω, and $.004 \times B_p \times J$ (where J = 1 to 14 or so) for σ_B. The other input quantities which control the orientation of the DD's are not relevant in this discussion, since the results are independent of this transformation.

When each individually generated DD is processed by the Sonnerup-Cahill MV program to determine the direction of minimum variation of the difference field vectors across the structure, the following ("noised-up") quantities are calculated:

B, which is $\sqrt{B_x^2 + B_y^2 + B_z^2}$ $(\approx \sqrt{B_n^2 + B_p^2})$, the total field magnitude (1)

$R = B_z/B$ (2)

$$\Delta R \equiv |\Delta B_z|/B, \text{ where } \Delta B_z = B_z - B_n \tag{3}$$

$$\beta = \cos^{-1}(|B_z|/B), \text{ the discontinuity cone angle,} \tag{4}$$

and

ω.

Also an average and rms deviation of these quantities are calculated over each 100 member set. ΔR_{max} is the quantity which ultimately must be estimated in order to separate TD's from RD's as discussed above. We now turn to some theoretical and speculative aspects of estimating ΔR and later shall relate them to the simulation results.

ESTIMATING ΔR-THEORETICAL

The average normal component of the field throughout the zone of the discontinuity can be expressed as

$$B_z = \vec{B} \cdot \hat{n} \tag{5}$$

where $\hat{n}$ is the unit vector normal to the discontinuity surface, and $\vec{B}$ is the average total field. The uncertainty in average B_z then is

$$dB_z = - B \sin\beta \; d\beta , \tag{6}$$

where $\vec{B}\cdot\hat{n} = B\cos\beta$ by the above definition of β, and where the average B is by prescription known exactly (to the accuracy of the measurements, a very small source of error). In the linear approximation we see that (where "T" refers to theoretical):

$$\Delta R_T \equiv \frac{|\Delta B_z|}{B} = |\sin\beta| \; |\Delta\beta| \tag{7}$$

We define α as the error in β, $\alpha = |\Delta\beta|$, and note that $|\sin\beta|$ is $\sin\beta$ since $0 < \beta < 90^{\circ}$ by choice of convenient coordinate system. Then

$$\Delta R_T = \alpha \sin\beta . \tag{8}$$

We speculate that α, although independent of β, will depend on ω

explicitly and on ω and σ_B implicitly through the eigenvalue ratios λ_1/λ_3 and λ_2/λ_3 whenever ΔR_T is calculated via the results of the MV method. The TD simulation studies (where $\beta = 90^\circ$) show that α (or ΔR_T) can be reasonably represented empirically by the product of two factors:

$$\alpha = 3/4 \; (\epsilon^{f(\omega)} \; \Lambda^{P}), \tag{9}$$

where $\Lambda = \lambda_3/\lambda_1 + \lambda_3/\lambda_2$, $P = 3.60 + 2.44 \log \Lambda$, and $f(\omega) = [(120^\circ-\omega)/120^\circ]^3$, for the ranges $30^\circ < \omega < 120^\circ$ and $0.18 < \Lambda < 1$ (the latter range translates to $1 < \lambda_2/\lambda_3 < 5.6$ for practical purposes). Figure 2 shows a plot of α (= ΔR_T for $\beta = 90^\circ$) for a restricted range of Λ of practical interest. For the above ranges ΔR_T is then

$$\Delta R_T = (3/4) \; [\exp(\frac{120^\circ-\omega}{120^\circ})^3] \; \sin\beta \; \Lambda^{(3.60 + 2.44 \log\Lambda)} \tag{10}$$

<u>for all DD's</u> on average, since α and β are presumably independent. As we will show in the next section, when $\lambda_2/\lambda_3 < 1.8$, the DD normal is too poorly determined to be useful. Therefore, we will be concerned only with the range $1.8 < \lambda_2/\lambda_3 < 5.6$ for the ΔR_T expression. For $\lambda_2/\lambda_3 > 5.6$ (or strictly $\Lambda < 0.18$) ΔR_T may be set equal to the left-most value of one of the curves in Figure 2, depending on the estimated ω.

SIMULATION RESULTS

In this section we present the results of the discontinuity simulation procedure, demonstrate why expression (10) for ΔR_T is a reasonable one for estimating ΔR_{calc} (= $|\Delta B_z|/B$), and discuss various features of ΔR_T.

Figure 3 shows how the resulting eigenvalue ratio λ_2/λ_3 varies as a function of the unperturbed discontinuity angle ω_T (i.e., true ω) and the dimensionless noise factor σ_B/B_p; each determined point is an average of 100 (=N) discontinuity simulations. Only the accentuated points are calculated values, and they are connected with straight line interpolations (Figures 3-9 contain this same simple interpolation scheme). As might be expected, this so called "mid-to-min" eigenvalue ratio increases dramatically as ω_1 increases for a fixed noise factor. Also, for a given ω_T, λ_2/λ_3 drops markedly as the noise factor is linearly increased. It should be stressed that each point in the figure holds for either a TD or an RD. For $\omega_T < 30^{\circ}$, λ_2/λ_3 is less than 1.8 for all but the lowest noise levels.

The λ_2/λ_3 ratio is an important statistical indicator of how well determined are the various physical properties of the discontinuity in question, e.g., ω, β, B_n and B_p. Obviously the lower the ratio λ_2/λ_3 is, the more poorly determined are these quantities on average, as we shall show. The eigenvalue ratio λ_1/λ_3 ("max-to-min") is usually considerably larger than λ_2/λ_3, sometimes by orders of magnitude. Therefore, λ_2/λ_3 is the ratio of greatest concern in an error analysis. (However, both λ_1/λ_3 and λ_2/λ_3 are important in pre-editing the events; more will be said on this in a later section.) Since the error associated with any quantity should depend on both λ_2/λ_3 and λ_1/λ_3, the empirical quantity Λ was set equal to $(\lambda_3/\lambda_1 + \lambda_3/\lambda_2)$; hence $\Lambda \sim \lambda_3/\lambda_2$. In the following figures the importance of λ_2/λ_3 in estimating the uncertainty associated with a quantity will become evident by a comparison with Figure 3.

In Figure 4 the calculated results for simulated average normal components as a function of ω_T and σ_B/B_p are given separately for RD's and TD's. The unperturbed B_p and B_n for these simulations are shown in the table in the figure. TD's and RD's throughout this study will be defined by this table. Since most of the quantities to be displayed are dimensionless, other values for B_p and B_n for the TD's are unnecessary, and of course for RD's an infinite set of B_n/B_p could be used; the characteristics chosen for the single unperturbed RD in the table were considered sufficient for our purposes. The circled points in the figure represent those for which the associated λ_2/λ_3 is < 1.7 (compare with Figure 3) and are usually associated with larger errors, as the figure shows. That is, they are markedly different from their unperturbed value B_n (0 or 5 nT) due to either a small ω_T or high noise factor σ_B/B_p. Notice that for a given ω_T and σ_B/B_p, B_n is, on average, more poorly estimated for TD's than for RD's. This is easily understood in terms of the simple geometrical factor $\sin\beta$ being proportional to the error in this case as indicated by equation (8) [strictly, the factor is $B \sin\beta$)]. Simulations show that indeed the difference between the error on B_n for TD's and RD's is proportional to $B \sin\beta$, especially for $30^\circ < \omega_T < 90^\circ$. Other simulations using B_n and B_p different from the values shown in the table in Figure 4 for RD's were performed with similar results. Table 1 gives rms deviations on B_z associated with the averages of $|B_z|$ of Figure 4. Notice the marked dependence of B_z-RMS on ω_T for small ω_T.

Directly related to B_z is the "cone angle" (i.e., the angle, β, that the normal makes with $\vec{B}$; see equation (4)). This depends on a dimensionless quantity, the ratio $|B_z|/B$. The results of the β simulations are shown in Figure 5. Our general comments on Figure 4 hold as well for this figure. Since $\cos^{-1}(5.0/5.59) = 26.6^\circ$, the point on the $\sigma_B/B_p = 0$ axis for RD's is at this value. Again the circled points, where $\lambda_2/\lambda_3 \leq 1.7$, are those for which large deviations in β from the ideal values of 90° (TD's) or 26.6° (RD's) are expected.

Figure 6 shows how the rms-deviations on β, associated with the averages displayed in Figure 4, vary with respect to ω_T, σ_B/B_p, and discontinuity type. Notice the strong dependence of β-RMS on σ_B/B_p for small ω_T, similar to the B_z-RMS behavior as shown in Table 1.

Figure 7 demonstrates how the simulated discontinuity angle ω, on average, varies as a function of ω_T and σ_B/B_p for RD's (solid curves) and TD's (dashed curves) separately. As expected, for large ω_T little variation occurs for all σ_B/B_p. As ω decreases or σ_B/B_p increases, deviations of ω increase significantly, especially for $\omega_T \leq 45^\circ$. Circled points are again those for which $\lambda_2/\lambda_3 \leq 1.7$. Oddly, the curve for RD's with $\omega_T = 20^\circ$ deviates little for most of the higher σ_B/B_p values even though the associated rms on each on these values is $\gtrsim 20^\circ$.

Figure 8 presents the rms deviation of ω as a function of σ_B/B_p for the ω_T's denoted for TD's and RD's separately corresponding to the averages shown in Figure 7. The parts of the curves representing useful simulations (i.e., $\lambda_2/\lambda_3 \geq 1.8$) obviously depend critically on ω_T for their rate of increase with increasing σ_B/B_p. A peculiar characteristic of these curves is their apparent independence of σ_B/B_p for the poor quality cases ($\lambda_2/\lambda_3 \leq 1.7$) for all ω_T, as if a "noise saturation" has been reached. Only for the largest ω_T's ($\gtrsim 90^\circ$) does ω-RMS remain relatively low ($\lesssim 11^\circ$) for the σ_B/B_p of interest.

Figure 9 shows ΔR_{calc} [$\equiv |B_z - B_n|/B$] as a function of ω_T and σ_B/B_p for TD's where $\lambda_2/\lambda_3 \geq 1.8$; all values of ΔR_{calc} for which $\lambda_2/\lambda_3 < 1.8$ were too high to be acceptable. The quantity ΔR_{calc} is important because it represents a measure of the estimated error on the normalized (by B) b_z component, and therefore is a proper parameter to use in judging whether a discontinuity is an RD or a TD, within the limitations dicussed in the Introduction. For a given noise factor σ_B/B_p (= 0.04 x J; J = 1,...14), ΔR_{calc}, on average, increases dramatically as ω_T decreases; the upper cut-offs, of course, are due to allowing only those cases for which $\lambda_2/\lambda_3 \geq 1.8$. Notice that there is little variation in the ΔR_{calc}'s between $\omega_T = 90^\circ$ and 120° for a given noise factor.

Figure 10 is similar to Figure 9, except now we consider RD's, and the ordinate scale is more sensitive by a factor of two; otherwise the same general comments hold. In comparing Figures 9 and 10, it is apparent that for a given set of ω_T and σ_B/B_p, ΔR_{calc} is, on average, consistent with our earlier comments concerning equation (8) and the $\sin\beta$ factor. Table 2 gives the ratio of the rms deviation of ΔR_{calc} to ΔR_{calc} itself associated with the averages of Figures 9 and 10. This ratio is not very sensitive to ω_T or σ_B/B_p, except that it becomes somewhat small for large ω_T for the TD cases.

A representative set of simulated RD's and TD's was used to calculate ΔR_{calc} in relation to ΔR_T (ΔR-"Theoretical") as given by equation (10) with $30^\circ \leq \omega_T \leq 120^\circ$, $\lambda_2/\lambda_3 \geq 1.8$, and $\Lambda \geq 0.18$ [the last restriction holds for a practical reason; it represents a lower bound on the applicability of equation (10)]. The results are shown in Figure 11. The TD's and RD's in general fall on the higher or lower portions of the curve, respectively. The data for the $\omega_T = 120^\circ$ cases would essentially cluster at the origin. This reasonably good agreement between ΔR_T and

ΔR_{calc} for rather broad ranges of ω_T and σ_b/B_p provides confidence that equation (10) is a useful and fairly reliable expression for estimating the error in B_z/B (i.e., ΔR_{calc}) for any discontinuity, RD or TD, after proper eigenvalue screening. For those TD's with $\Lambda < 0.18$, a conservative value for ΔR_T could simply be one taken from the left most limit of one of the curves in Figure 2 according to the estimated ω; for RD's, this value should be multiplied by $\sin\beta$, where β is an estimated angle.

Equation (10) for TD's was empirically generated by a trial-and-error examination of various functions of Λ alone. After a reasonably satisfactory one was derived, it was noted that a correction factor $f(\omega)$ was necessary to account for disproportionately large errors at small ω. The factor $\sin\beta$ was then incorporated to account for a finite normal component in the case of RD's, as discussed above, and simulations showed that to be an appropriate tack. Figure 12 demonstrates the steep rise in the ω-correction factor that was necessary for small ω. Equation (10) comprises only five fixed constants and depends on only three input quantities, one (Λ) known exactly by prescription and two (ω and β) estimated by the MV technique. How well ω and β are estimated will also depend on λ_2/λ_3. Regardless of this interdependence of input quantities, Figure 11 shows that, on average, ΔR_T is a good approximation to ΔR_{calc}.

Using actual discontinuity data from the Mariner 10 magnetic field experiment (Lepping and Behannon, 1979), we generated ΔR_T percent-distributions by employing the MV technique and equation (10). This was carried out for three different locations of the spacecraft from the sun: 1.00 A.U. (163 DD's), 0.72 A.U. (206 DD's), and 0.46 A.U. (275 DD's). The results are shown in Figure 13. Notice that the distributions sharply peak at 0.015. Also note that about 86% of the Mariner 10 ΔR_T distributions individually lie in the range $0.0 \leq \Delta R_T \leq 0.06$; strictly speaking, 86% is a weighted (by N) average of the percentages 88.7, 84.8, and 83.0 for the 0.46, 0.72, and 1.0 AU positions, respectively. So $\Delta R_T = 0.06$ could be chosen as a useful maximum relative error on $|B_z|$ for the entire Mariner 10 data set by definition, realizing that it holds quite well for <u>each location</u> individually. To be conservative, we choose to define a "cut-off" shown in the figure, which is twice that value. Hence, $\Delta R_{1,cut\text{-}off} = 0.12$, which incidentally is nearly a true upper bound on each of the entire three distributions. Choosing a cut-off to be twice the ΔR_1 of 68% is motivated by the fact that the errors associated with the most probable $|B_z|$ errors are themselves sometimes comparable in magnitude as indicated in Table 2, which displays the related relative RMS (ΔR_{calc}). For purpose of error interpretation we now convert the cut-off estimation, which is a mean deviation, to an equivalent standard deviation.

Specifically, it is useful to estimate what this cut-off is when expressed as twice a standard deviation (for a relative error at 95% certainty). Recognizing that $\langle \Delta R_{calc} \rangle$ is a mean deviation and assuming that the ΔR_{calc}-distribution is probably well approximated as normal, and was in fact modeled that way, we immediately see that

$$\langle \Delta R_{calc} \rangle = \sqrt{\frac{2}{\pi}}\, \sigma_{calc} = 0.7979\, \sigma_{calc} \tag{11}$$

or

$$2\,\sigma_1 \lesssim \frac{2\,\langle \Delta R_1 \rangle}{0.7979}\,, \tag{12}$$

where the "calculated" quantities are replaced by "theoretical" ones, justified again by the results shown in Figure 10. Using the cut-off value of $\langle \Delta R_1 \rangle_{max}$ of 0.12 we obtain the maximum $2\text{-}\sigma_1$ value of

$$2\,\sigma_{max} \lesssim 0.301. \tag{13}$$

Since an ideal TD has a B_z component of zero, then, to a certainty greater than $\lesssim$ 95%, the identified TD's may appear to have errors as large as 0.30 in $|B_z|/B$ according to this error analysis, where in this case $\Delta B_z = B_z$. Conversely, all DD's whose $|\Delta B_z|/B$ exceeds 0.30 are, with $\lesssim$95% certainty, RD's.

This max-ΔR can be translated into a max-β [see equation (4)], i.e., the largest reasonable cone angle below which the DD is 95% likely to be an RD and above which it is probably a TD (but with much less certainty without further analysis). This cut-off cone angle is

$$\beta_{max} = \cos^{-1}(0.301) = 72.5^{\circ}. \tag{14}$$

This criterion was used as a first discriminator between TD's and RD's in the analysis of Mariner 10 data at 1 A.U.

APPLICATION OF THE METHOD

Figure 14 shows the relationship between σ_F/F and the cone angle β for the 163 DD's identified in the Mariner 10 interplanetary magnetic field data at 1 A.U. for the period 4-17 November 1973, where F is the average magnetic field magnitude across a DD and σ_F is the associated standard deviation; σ_F/F then is a relative magnitude noise factor. Obviously σ_F/F is unrestricted for TD's but must be small (chosen here arbitrarily to be ≤ 0.09) for RD's. The vertical line at $\beta = 72.5^{\circ}$ marks the upper limit on RD's as discussed above. The RD's falling in the top-left box (n = 10) are interpreted to be low quality RD's and are therefore dismissed from further consideration. The bottom-left box (n = 62) contains good quality RD's. The top-right box (n = 29) includes TD's that are probably of good quality in that such large σ_F/F values would not permit their identification as RD's for large β's. The bottom-right box (n = 62) is, strictly speaking, a mixed RD-TD set, but study (Burlaga, 1971) shows that it probably is comprised mainly of TD's. It is not unreasonable to estimate the ratio of TD's to RD's to be

$$\text{Ratio (TD/RD)} \approx \frac{29 + 62}{62} = 1.5$$

at 1 A.U. in early November 1973. This ratio is obviously a very variable quantity in general as other studies have shown (Burlaga et al., 1977; Solodyna et al., 1977). Various characteristics of the RD's and TD's in Figure 14 are described elsewhere (Lepping and Behannon, 1979).

The use of β as a discriminator of DD type requires that β be reliably estimated in all cases ultimately included in the statistics. In order to ascertain the confidence one can place on β from Equation (4) for an individual DD, the error in β can be estimated by use of equations (10) and (12), where $< \Delta R_T > \rightarrow \Delta R_T$.

FURTHER CONSIDERATIONS: FIELD MAGNITUDE CHANGE WITHIN DD'S

As was stated in the introduction, no attempt was made in this simulation study to model "exotic" types of directional discontinuities, such as magnetic holes, in which there is a very large dip in field magnitude associated with the DD. Recently, however, Fitzenreiter (1979) has suggested that even cases with relatively modest dips in B can produce serious errors in the Sonnerup-Cahill minimum variance analysis and possibly even lead to a misidentification of a DD as an RD when it is in fact a TD. These conclusions are based on results of analysis of interplanetary DD's using both minimum variance analysis and a two-spacecraft technique to identify the DD type.

This suggestion prompted the modification of the simulation program to include a smooth, continuous dip in the field magnitude from a given maximum at the end points of the generated time series to a minimum at an angle $\omega_F/2$, where ω_F is the full rotation angle across the DD in the discontinuity plane. The problem alluded to by Fitzenreiter is one in which the field magnitude dips in such a way that it results in a hodograph, or trace produced by the tip of the rotating vector in the plane of the discontinuity, that is nearly a straight line. If it <u>is</u> a straight line then there is a degeneracy in the MV calculation; in the absence of asymmetric noise contributions the intermediate and minimum eigenvalues, λ_2 and λ_3, are both zero. Obviously when this condition is approached, errors associated with the minimum variance solution increase.

The size of the magnitude dip which leads to degeneracy in a given case is a function of the angle ω_F. For a straight-line hodograph it is easily shown that the field magnitude varies across the DD according to

$$B_i = \frac{\cos(\omega_F/2)}{\cos(\omega_F/2 - \omega_i)} B_o, \tag{15}$$

where B_o is the unperturbed field magnitude outside the discontinuity (and at the boundaries), and B_i and ω_i (where $0 \leq \omega_i \leq \omega_F$) correspond to the magnitude and angle associated with the ith field vector within the DD. At the center then (where $\omega_i = \omega_F/2$), the minimum field is simply $B_{min} = (\cos \omega_F/2)\ B_o$. In this new simulation study a range of ω_F values is considered, where for each ω_F a series of dips in magnitude are simulated corresponding to varying fractions of the dip amplitude which would give degeneracy. In addition, the various cases are repeated for a series of "noise factors" within a range that includes the values previously used in the constant vector magnitude study.

In the absence of noise, equation (15) tells us that for ω_F angles of 30^o, 60^o and 90^o, degeneracy in the Sonnerup-Cahill MV analysis results for $\Delta B_{max}/B_o$ = 0.034, 0.134 and 0.293, respectively, where $\Delta B_{max} = B_o - B_{min}$. The first two values are relatively modest decreases in field magnitude which are not uncommon among interplanetary discontinuities, where a rigorously constant field magnitude is seldom observed.

The preliminary results of the study indicate that the problem is made more acute by the addition of noise, as would be expected. As a worse case situation, we have considered what conditions are required to produce an error in the identification of DD type, i.e., for a simulated TD with a dip in B to be misinterpreted as an RD as a result of $|\Delta B_z|/B$ estimated from the minimum variance analysis exceeding 0.30. It was found that at $\omega_F = 60^o$ for a moderate noise factor of 0.017, corresponding to an rms noise amplitude of 0.1 nT, the critical error would occur for a dip greater than 80% of $\Delta B_{max}/B_o$ (> 0.107) and at $\omega_F = 30^o$ for a dip greater than 30% of $\Delta B_{max}/B_o$ (> 0.010). In these cases a value of B_o = 6 nT was used.

The encouraging aspect of these preliminary studies, however, is that in almost every case of an incorrect interpretation of a TD as an RD, the eigenvalue ratio λ_2/λ_3 was less than 2.0. Thus, use of that value as a minimum allowed value of λ_2/λ_3 appears to be a sufficient criterion in the majority of cases to at least prevent incorrect interpretation, although varying degrees of error will still occur in the estimation of the magnitude and direction of the normal. Those cases in which the criterion did not work (less than 10% of the total cases studied) were cases with $\omega_F < 40^\circ$. Hence elimination of such small angle cases in addition to the λ_2/λ_3 criterion would prevent this most critical error from occurring.

It is probable that an additional indicator of "nearness-to-degeneracy" is provided by the ratio λ_1/λ_2. How large it can be is a function of the level of noise present. For a noise amplitude of 0.1 nT a reasonable criterion may be $\lambda_1/\lambda_2 < 100$. This is currently the subject of continuing investigation. The establishment of tighter error limits on the estimation of the normal will undoubtedly reduce that upper limit. On the other hand, a limiting value of 100 may be unnecessarily low for very clean cases in which the ambient noise level is exceedingly low. Future simulation study should shed more light on such considerations and more generally on the question of the errors associated with the use of the Sonnerup-Cahill MV analysis for studying DD's that include magnitude dips. An additional aspect being studied is the effect of dips whose amplitude exceeds that which gives degeneracy. The results of this simulation study, together with examples drawn from DD's observed in the interplanetary magnetic field, will be discussed in a future report.

SUMMARY AND DISCUSSION

We have statistically investigated the errors associated with a minimum variance analysis (Sonnerup and Cahill, 1967) of DD's by use of an idealized model of these discontinuities and various simulations, and also by an examination of actual Mariner 10 IMF data. An empirical expression for the magnitude of the error in an estimated discontinuity normal component, relative to the total field across the DD (or alternately the error in β, the cone angle), was derived, as well as other relevant statistical properties. Application of this formula to a total of 644 Mariner 10 discontinuities has provided a more precise but probably conservatively estimated upper bound of 72.5° on the cone angle β (Equation (4)) for rotational discontinuities in separating RD's from TD's in studies using only magnetic field data from a single spacecraft.

In carrying out the simulations in this study, the range $0.0 \leq \sigma_B/B_p \leq 0.056$ was considered a reasonable extent for the "noise" factor. This choice was made because the resulting simulated DD characteristics, the λ-ratios in particular, correspond on average to those found in typical interplanetary DD analyses (Lepping and Behannon, 1979).

The simulation study is believed to be an important first step in understanding the figure of merit one should place on such minimum variance analyses of the magnetic field, but it should be pointed out that the simulations were implemented by use of an isotropic (random) noise generator. In actuality a systematic, though usually small, three dimensional perturbation may be superimposed upon what may be viewed as a randomly "noised-up" discontinuity. Such perturbations are occasionally wave-like fluctuations and are markedly nonlinear. Also, some TD's can have rather large σ_F/F values, as Figure 14 shows, which is mainly due to "B_p" changing considerably through the discontinuity zone. (In most instances, however, as Figure 14 also shows, most DD's in general have values of σ_F/F which fall below 0.09.) These additional perturbations which have not been modeled here will contribute to the error on the estimate normal direction (Δβ) and on the B_z component (and on the resulting estimated ω). Since this study has attempted to develop conservative estimates, i.e., reasonable upper limits, it is believed that some of these nonlinear and anisotropic effects are covered, but further study addressing these issues is probably warranted, especially a study (briefly covered here) on <u>magnitude</u> dips within the DD.

It should also be pointed out that even in those cases where the DD can be well approximated as an idealized DD plus superimposed isotropic noise, the resulting error "cone" angle Δβ is not usually azimuthally symmetric about $\hat{n}$. That is, the directional error is larger in the m_2-m_3 plane than in the m_1-m_3 plane, since λ_1/λ_3 is usually much larger than λ_2/λ_3, where m_1, m_2, and m_3 are the eigenvector directions associated with the true maximum, intermediate, and minimum eigenvalues, respectively. This is a simple geometrical fact which is dependent on the eigenvalue ratios and the size of ω (Sonnerup, 1971). By our choice of $\beta = \cos^{-1}(|B_z|/B)$, we have in effect isotropized the cone angle for simplicity, as well.

This analysis was performed principally to aid in differentiating between the interplanetary TD's and RD's observed by Mariner 10 as part of a study to appear as a future paper. However, the analysis developed for this DD error study should have fairly broad application in other similar studies, including the analysis of magnetopause normal errors.

ACKNOWLEDGMENTS

We are very grateful to L. F. Burlaga for helpful suggestions through the course of this work and for reading the manuscript. We thank K. W. Ogilvie for initially encouraging us to examine the issues addressed by this work and D. Howell and P. Harrison for the Mariner 10 data processing effort.

REFERENCES

Burlaga, L. F., Directional discontinuities in the interplanetary magnetic field, Solar Phys., 7, 54, 1969.

Burlaga, L. F., On the nature and origin of directional discontinuities, J. Geophys. Res., 76, 4360, 1971.

Burlaga, L. F., J. F. Lemaire, and J. M. Turner, Interplanetary current sheets at 1 A.U., J. Geophys. Res., 82, 3191, 1977.

Denskat, K. U. and L. F. Burlaga, Multispacecraft observations of microscale fluctuations in the solar wind, J. Geophys. Res., 82, 2693, 1977.

Fitzenreiter, R. J., Two-spacecraft measurements of the structure of tangential discontinuities, EOS, Transactions A.G.U., 60,(SS23), 365, 1979.

Hudson, P. D., Discontinuities in an anisotropic plasma and their identification in the solar wind, Planet. Space Sci., 18, 1611, 1970.

Ivanov, K. G., Rotational discontinuities in the solar wind, Akademia nauk SSR, Institut zemnogo magnetizma, ionosfery i rasprostraneniya radiovoln, Moscow, 1970, NASA Technical Translation, GSFC 1.5, September 1970.

Lepping, R. P. and K. W. Behannon, Magnetic field directional discontinuites: 2. characteristics between 0.46 and 1.0 AU, in preparation, 1979.

Siscoe, G. L., Discontinuities in the solar wind, Solar Wind Three, ed. C. T. Russell, p. 150, University of California Press, Los Angeles, 1974.

Siscoe, G. L., L. Davis, Jr., P. J. Coleman, Jr., E. J. Smith and D. C. Jones, Power spectra and discontinuities of the interplanetary magnetic field: Mariner 4, J. Geophys. Res., 73, 61, 1968.

Smith, E. J., Identification of interplanetary tangential and rotational discontinuities, J. Geophys. Res., 78, 2054, 1973a.

Smith, E. J., Observed properties of interplanetary rotational discontinuities, J. Geophys. Res., 78, 2088, 1973b.

Solodyna, C. V., J. W. Sari and J. W. Belcher, Plasma field characteristics of directional discontinuities in the interplanetary medium, J. Geophys. Res., 82, 10, 1977.

Sonnerup, B.U.O., Magnetopause structure during the magnetic storm of September 24, 1961, J. Geophys. Res., 76, 6719, 1971.

Sonnerup, B.U.O., and L. J. Cahill, Magnetopause structure and attitude from Explorer 12 observations, J. Geophys. Res., 72 171, 1967.

Tsurutani, B. T., and E. J. Smith, Interplanetary discontinuities: temporal variations and the radial gradient from 1 to 8.5 AU, to appear in *J. Geophys. Res.*, 1979.

Turner, J. M., L. F. Burlaga, N. F. Ness, and J. F. Lemaire, Magnetic holes in the solar wind, *J. Geophys. Res.*, *82*, 1921, 1977.

Turner, J. M., and G. L. Siscoe, Orientations of rotational and tangential discontinuities in the solar wind, *J. Geophys. Res.*, *76*, 1816, 1971.

TABLE 1

B_z-RMS (in nT)

$(\lambda_2/\lambda_3 \geq 1.8$ for cases above dashed line)

σ_B/B_p \ ω_T	TD 20°	TD 30°	TD 45°	TD 60°	TD 90°	TD 120°	RD 20°	RD 30°	RD 45°	RD 60°	RD 90°	RD 120°
.004	0.65	0.13	0.06	0.03	0.01	0.00	0.51	0.13	0.05	0.02	0.01	0.00
.008	1.64	0.45	0.14	0.06	0.01	0.00	1.57	0.34	0.10	0.05	0.02	0.01
.012	1.77	1.02	0.23	0.10	0.02	0.01	1.59	0.61	0.17	0.08	0.03	0.01
.016	1.80	1.36	0.31	0.13	0.02	0.01	1.64	1.19	0.24	0.10	0.03	0.02
.020	1.62	1.66	0.43	0.22	0.04	0.01	1.66	1.64	0.35	0.15	0.04	0.02
.024	1.60	1.72	0.61	0.18	0.04	0.01	1.65	1.62	0.40	0.15	0.05	0.03
.028		1.52	0.91	0.28	0.06	0.01		1.69	0.73	0.23	0.07	0.03
.032		1.70	0.88	0.30	0.06	0.02		1.49	0.78	0.23	0.08	0.03
.036		1.71	1.30	0.37	0.06	0.02		1.66	1.03	0.31	0.08	0.03
.040		1.79	1.48	0.47	0.10	0.02		1.56	1.40	0.35	0.10	0.04
.044		1.76	1.41	0.45	0.08	0.03		1.71	1.26	0.36	0.09	0.04
.048		1.62	1.42	0.71	0.11	0.02		1.77	1.22	0.56	0.11	0.04
.052		1.70	1.60	0.75	0.11	0.03		1.52	1.56	0.74	0.13	0.05
.056	1.70	1.74	1.68	0.89	0.13	0.02	1.71	1.89	1.28	0.62	0.15	0.05

TABLE 2

$RMS\{\Delta R_{calc}\}/<\Delta R_{calc}>$

($\lambda_2/\lambda_3 \geq 1.8$ for cases above dashed line)

σ_B/B_p \ ω_T	TD 20°	TD 30°	TD 45°	TD 60°	TD 90°	TD 120°	RD 20°	RD 30°	RD 45°	RD 60°	RD 90°	RD 120°
.004	.69	.76	.68	.60	.27	.10	.76	.76	.70	.73	.82	.80
.008	.66	.71	.74	.66	.27	.09	1.15	.75	.78	.81	.71	.80
.012	.64	.80	.70	.61	.28	.08	1.05	.87	.73	.73	.67	.73
.016	.53	.71	.71	.66	.26	.13	.94	1.18	.74	.80	.74	.80
.020	.48	.61	.75	.77	.31	.11	.97	.99	.91	.84	.70	.72
.024	.46	.58	.81	.61	.31	.11	.90	.99	.84	.69	.76	.74
.028		.53	.82	.63	.37	.10		.95	1.08	.72	.74	.79
.032		.62	.77	.69	.33	.11		1.03	1.10	.77	.69	.76
.036		.52	.81	.65	.26	.09		1.01	1.27	.90	.73	.78
.040		.58	.79	.68	.37	.11		1.01	1.14	.74	.78	.74
.044		.58	.70	.70	.32	.12		.99	1.02	.89	.83	.82
.048		.49	.84	.75	.38	.11		.91	1.24	.96	.88	.71
.052		.53	.70	.75	.34	.10		1.05	1.28	1.22	.72	.80
.056	.46	.54	.70	.79	.35	.09	.80	.91	1.02	.93	.74	.70

FIGURE CAPTIONS

Figure 1. Schematic representation of an ideal DD. For a TD B_n is zero; all other DD's are RD's. The subscript T refers here to the true or unperturbed coordinate system. All other symbols are defined in the text.

Figure 2. Derived theoretical (T) relationship between the relative normal error $\Delta \hat{R}_1$ (= $|\Delta B_z|/B$) and a composite eigenvalue "ratio" Λ for TD's (i.e., $\beta = 90^\circ$) at various discontinuity angles ω.

Figure 3. Eigenvalue ratio λ_2/λ_3 as a function of relative noise factor σ_B/B_p for various input ω_T's.

Figure 4. Average of normal magnitude $|B_n|$ as a function of relative noise factor for various input ω_T's for RD's and TD's. Table shows the "true" input characteristics for the RD's and TD's used in the simulation for this and the next 7 figures. The averages are taken over N = 100 simulations for each point in this figure. Unacceptable averages, where λ_2/λ_3 was ≤ 1.7, are shown for completeness.

Figure 5. Average of normal (or cone) angle β as a function of relative noise factor for various ω_T's for RD's and TD's.

Figure 6. The rms values of β associated with the average β's of Figure 5 for the same conditions.

Figure 7. Average discontinuity angle ω as a function of relative noise factor for various ω_T's for RD's and TD's.

Figure 8. The rms values of ω associated with the average ω's of Figure 7 for the same conditions. Notice that all those with $\lambda_2/\lambda_3 \leq 1.7$, shown by open circles, are unacceptable DD's and are given only for completeness.

Figure 9. The (calculated) average relative normal magnitude error as a

function of ω_T for various relative noise levels $J = 1, \ldots 14$ for TD's.

Figure 10. Similar to Figure 9 but now for RD's.

Figure 11. A comparison of theoretical and calculated relative normal magnitude errors for various ω's. Notice that as ω increases both ΔR_T and ΔR_{calc} tend to decrease, as expected.

Figure 12. Empirical relationship $f(\omega)$ showing how relative normal magnitude errors vary as a function of ω for all other characteristics held constant. See text.

Figure 13. ΔR_T distributions based on Mariner 10 magnetic field data from the three locations listed and using the defining equation (10). Lepping and Behannon (1979) discuss the data sets. Nearly 100% of the distributions lie between 0 and the cut-off at 0.12.

Figure 14. Scatter diagram of Mariner 10 discontinuity data at 1.0 AU showing relative magnitude rms deviation σ_F/F (from measurements across the DD zone) as a function of β. See text. The arrows and numbers at the top-right, just outside the box, represent in all cases but one (.260) legitimate TD's whose σ_F/F was too large to plot.

IDEALIZED DIRECTIONAL DISCONTINUITY

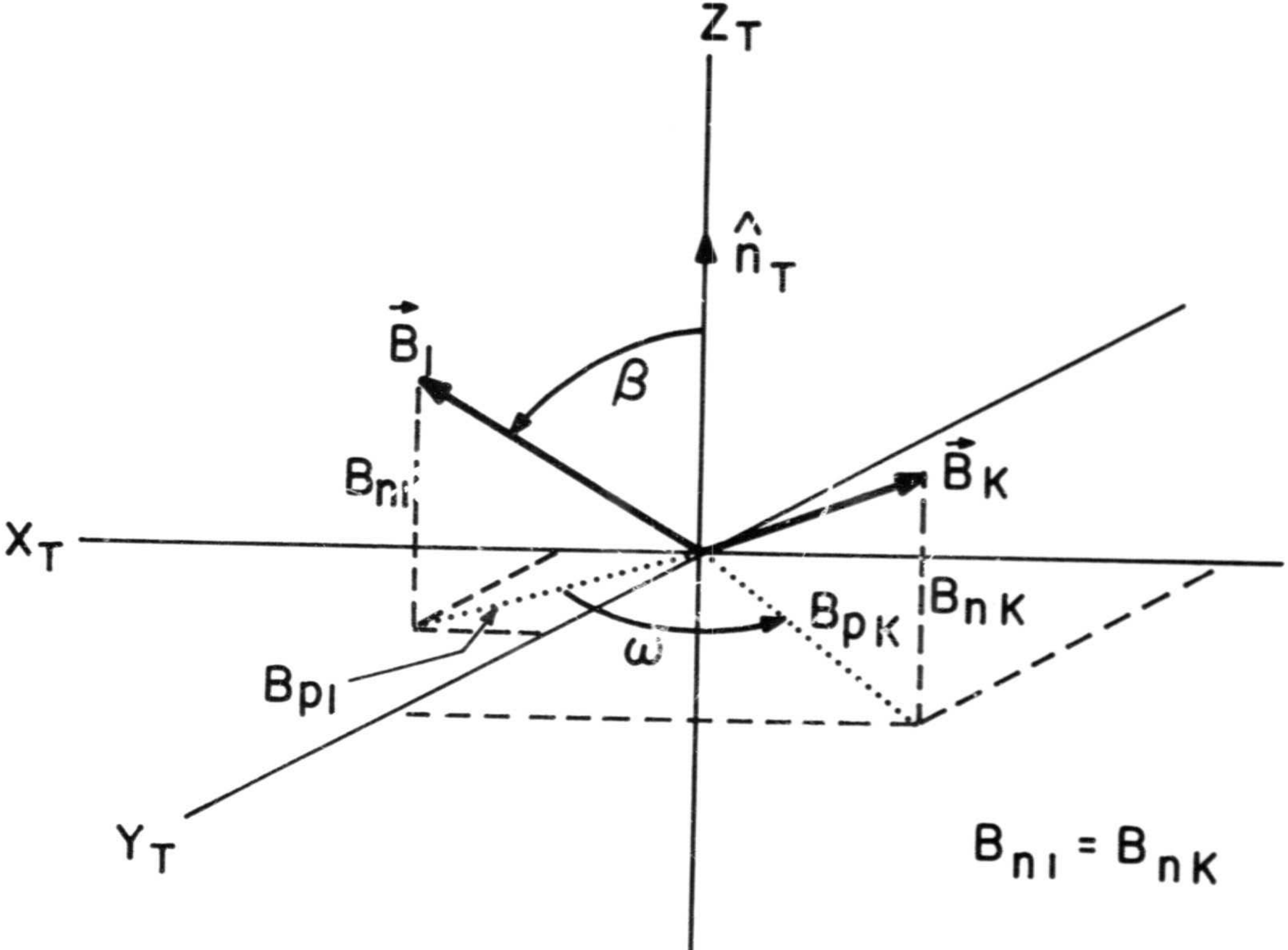

Figure 1

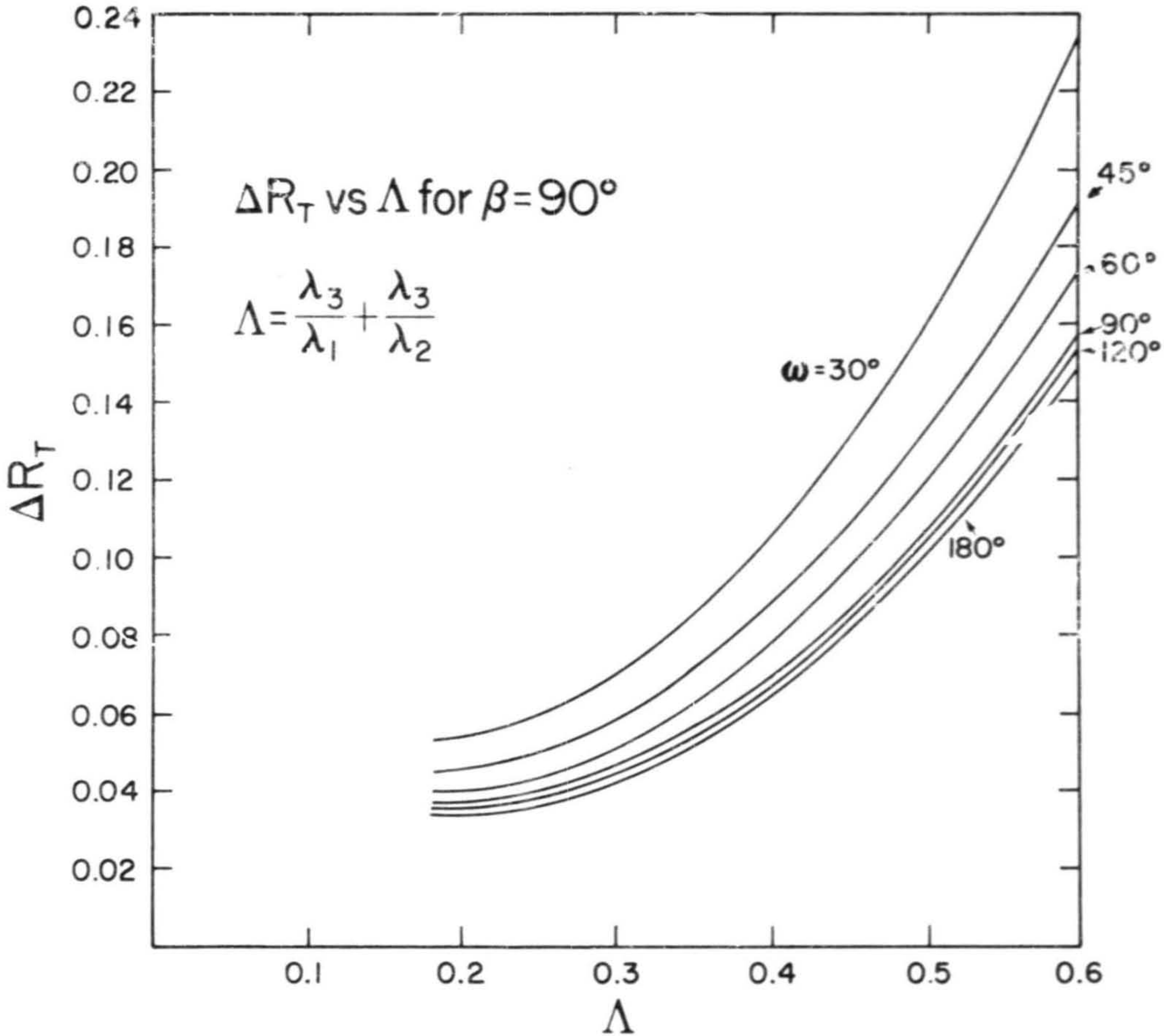

ΔR_T vs Λ for β=90°
Λ = λ3/λ1 + λ3/λ2
ω=30°
45°
60°
90°
120°
180°
ΔR_T
Λ
0.24
0.22
0.20
0.18
0.16
0.14
0.12
0.10
0.08
0.06
0.04
0.02
0.1
0.2
0.3
0.4
0.5
0.6

Figure 2

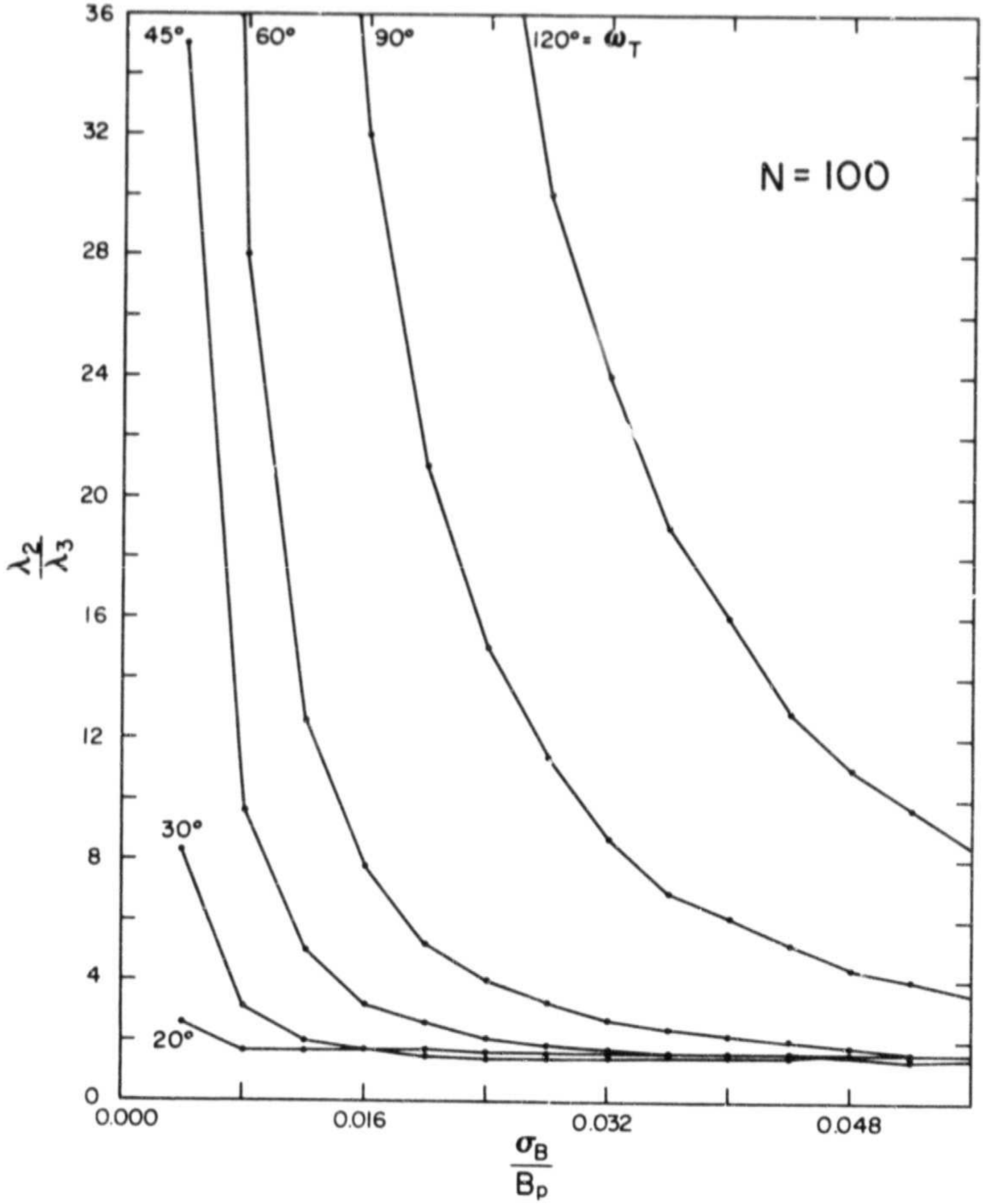

36
32
28
24
20
16
12
8
4
0
45°
60°
90°
120° = ω_T
N = 100
30°
20°
$\frac{\lambda_2}{\lambda_3}$
0.000
0.016
0.032
0.048
$\frac{\sigma_B}{B_p}$

Figure 3

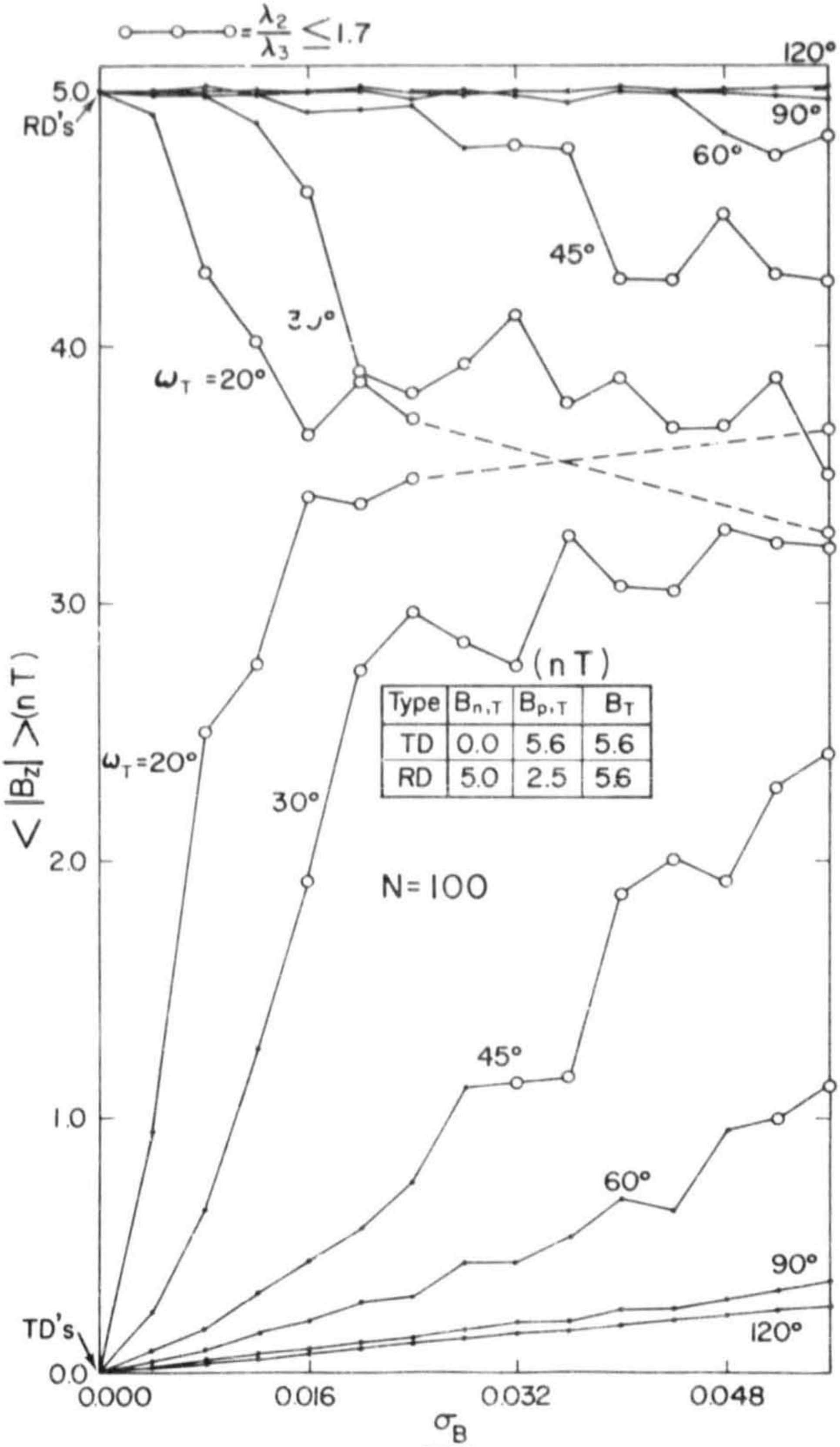

$\lambda_2/\lambda_3 \leq 1.7$
120°
90°
60°
45°
30°
ω_T =20°
RD's
TD's
$< |B_z| >$ (n T)
σ_B / B_p
(n T)
Type	$B_{n,T}$	$B_{p,T}$	B_T
TD	0.0	5.6	5.6
RD	5.0	2.5	5.6
N=100

Figure 4

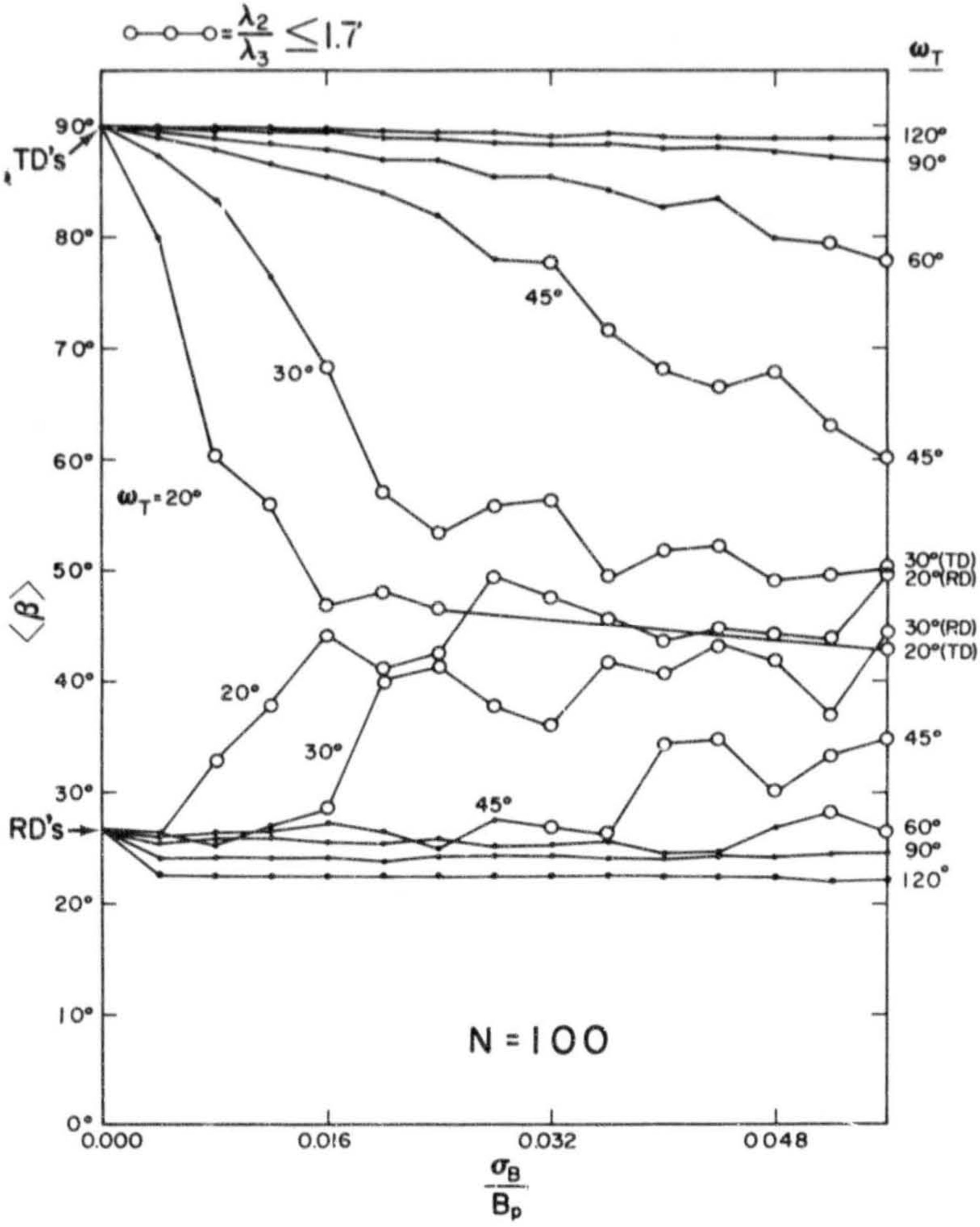

$\circ\!-\!\circ\!-\!\circ = \frac{\lambda_2}{\lambda_3} \leq 1.7$
ω_T
90°
TD's
80°
70°
60°
50°
40°
30°
RD's
20°
10°
0°
$\langle\beta\rangle$
0.000
0.016
0.032
0.048
$\frac{\sigma_B}{B_p}$
120°
90°
60°
45°
30°(TD)
20°(RD)
30°(RD)
20°(TD)
45°
60°
90°
120°
45°
30°
$\omega_T = 20°$
20°
30°
45°
N = 100

Figure 5

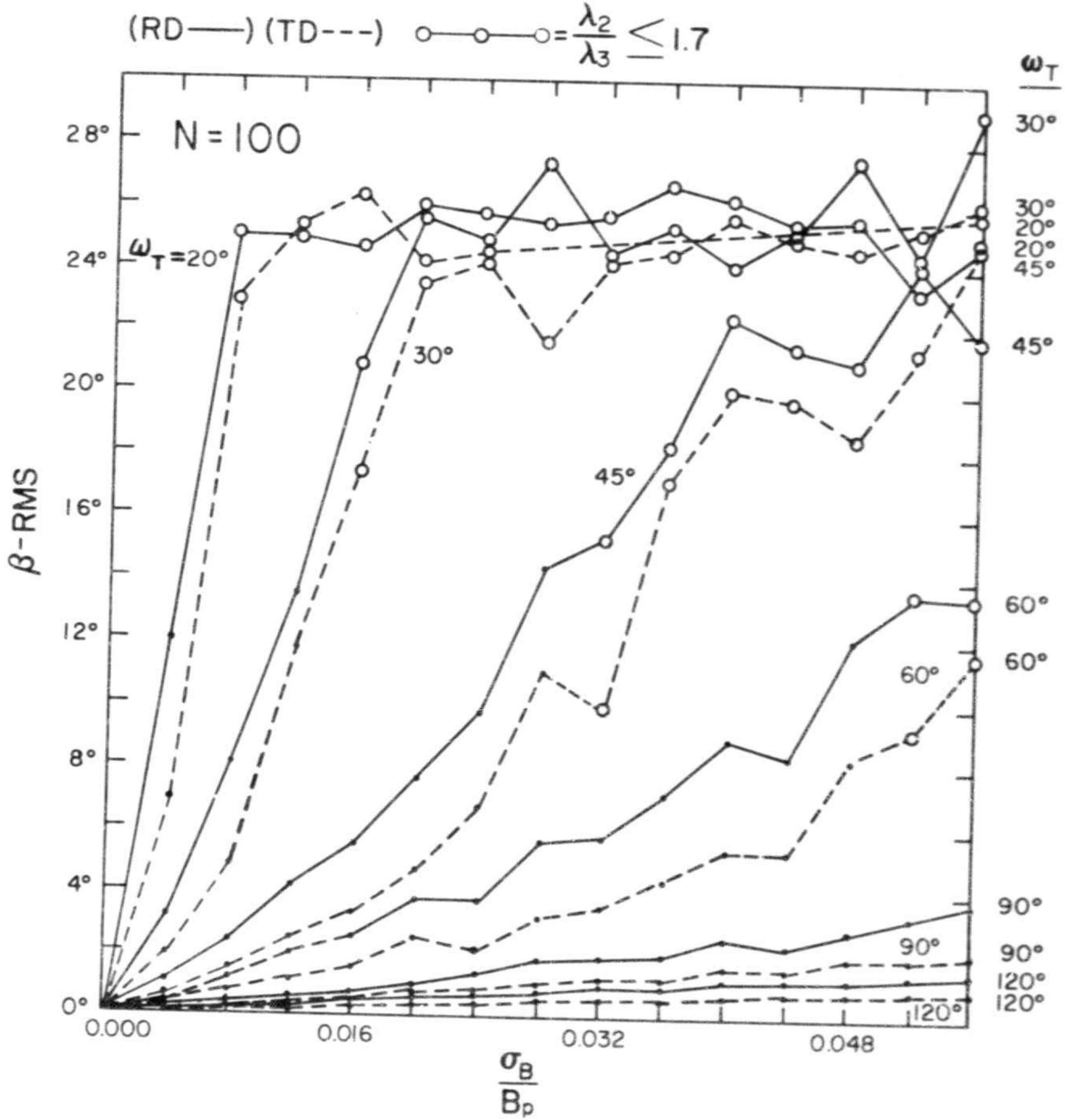

(RD——) (TD---) o—o—o = $\frac{\lambda_2}{\lambda_3} \leq 1.7$
N = 100
ω_T
$\omega_T = 20°$
30°
45°
60°
90°
120°
β-RMS
28°
24°
20°
16°
12°
8°
4°
0°
0.000
0.016
0.032
0.048
$\frac{\sigma_B}{B_p}$

Figure 6

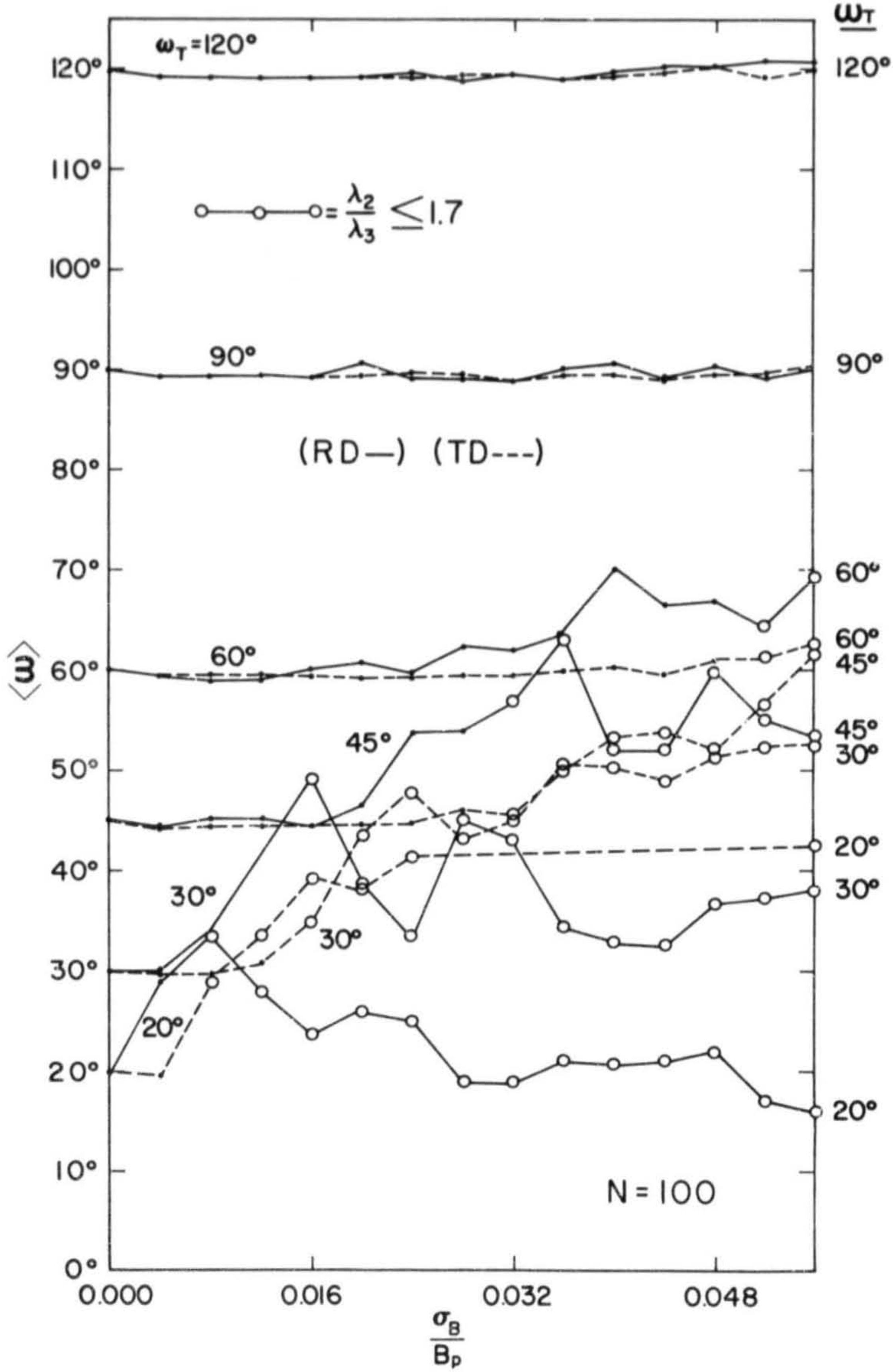

ω_T
$\omega_T = 120°$
120°
110°
100°
90°
80°
70°
60°
50°
40°
30°
20°
10°
0°
$=\frac{\lambda_2}{\lambda_3} \leq 1.7$
(RD—) (TD---)
45°
30°
N = 100
$\langle\omega\rangle$
0.000
0.016
0.032
0.048
$\frac{\sigma_B}{B_p}$

Figure 7

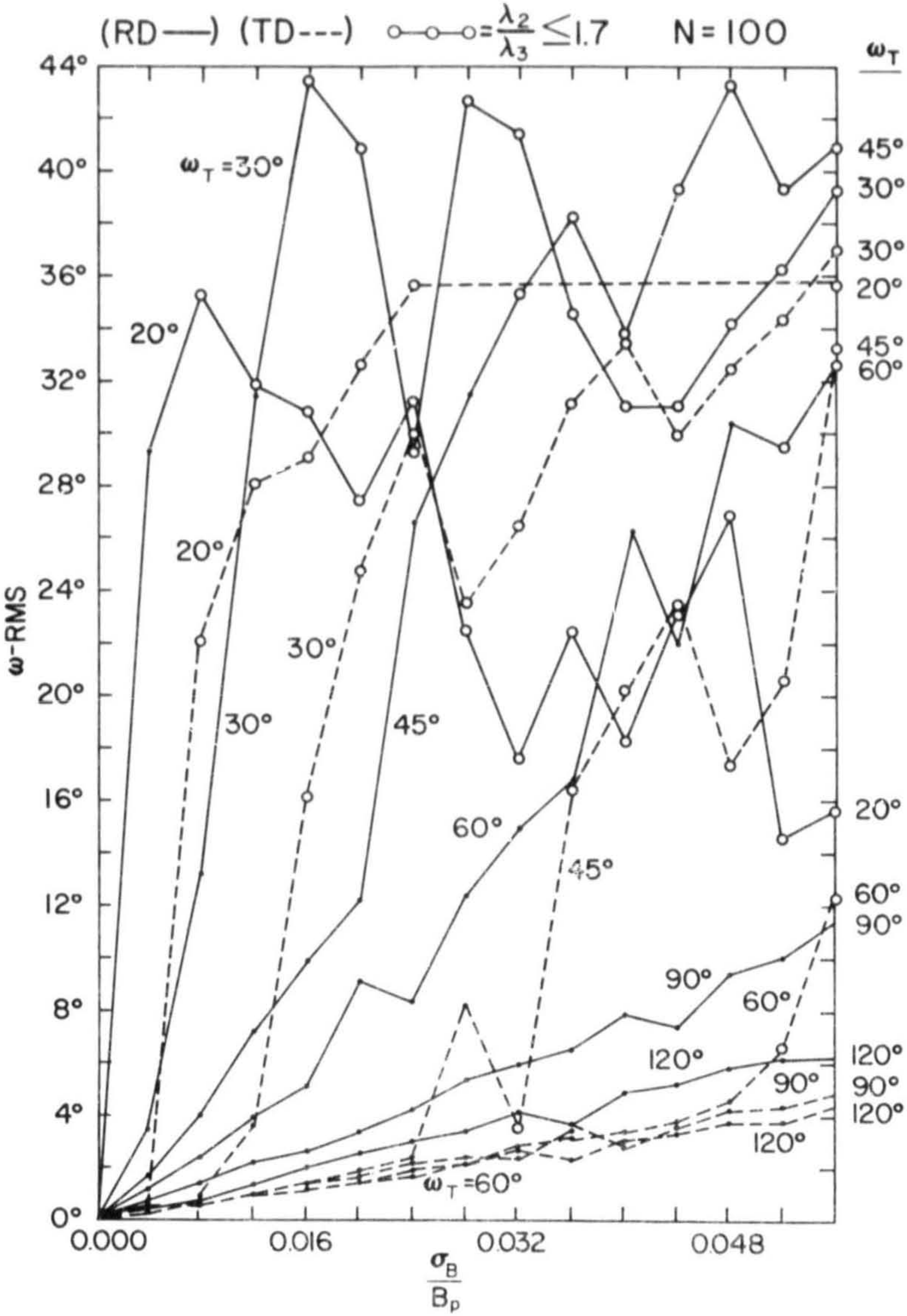
(RD ——) (TD - - -) o—o—o = $\frac{\lambda_2}{\lambda_3} \leq 1.7$ N = 100
ω_T
ω-RMS
$\frac{\sigma_B}{B_p}$
0.000
0.016
0.032
0.048
0°
4°
8°
12°
16°
20°
24°
28°
32°
36°
40°
44°
ω_T = 30°
20°
20°
30°
30°
45°
60°
45°
90°
60°
120°
90°
120°
ω_T = 60°
45°
30°
30°
20°
45°
60°
20°
60°
90°
120°
90°
120°

Figure 8

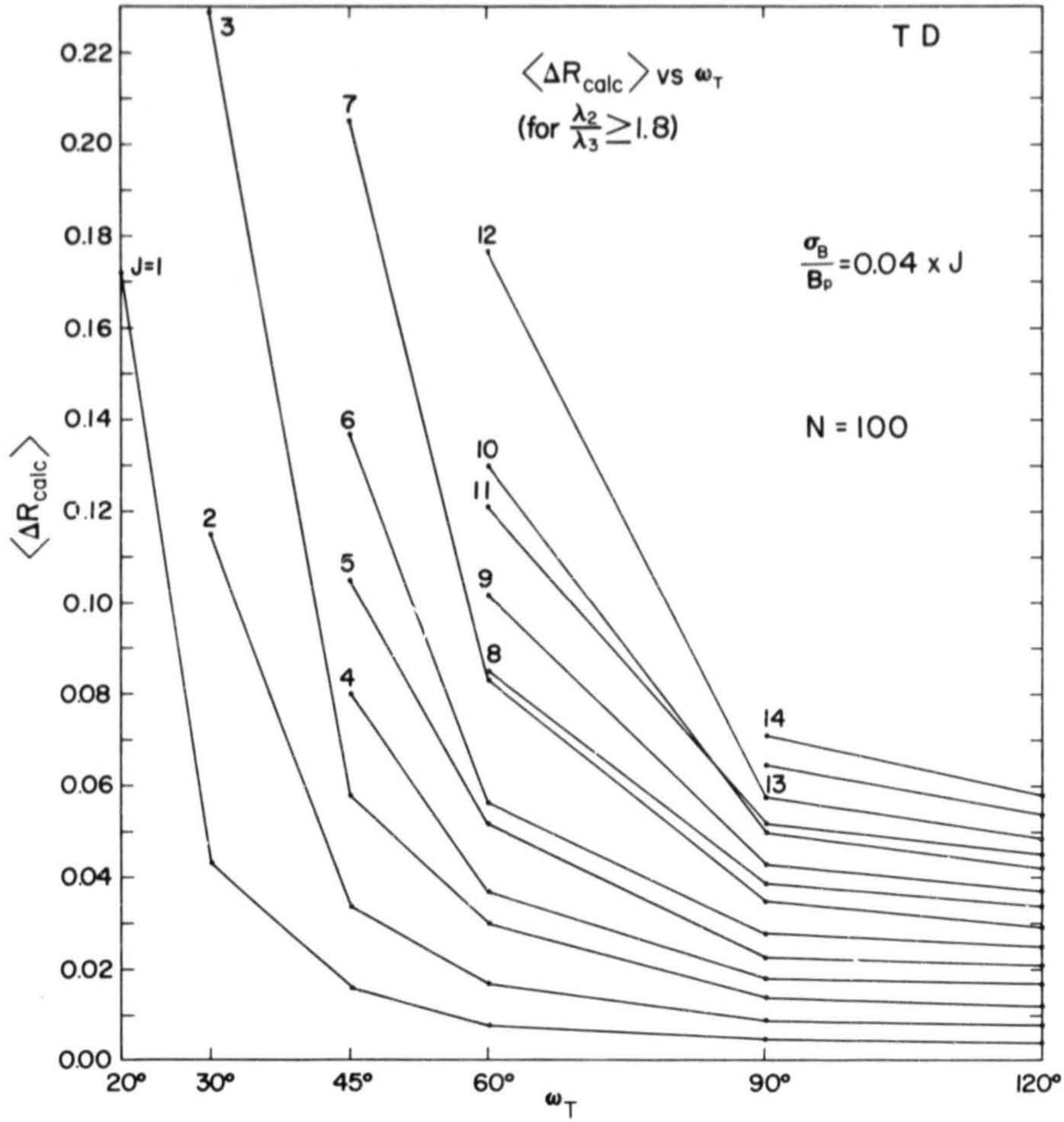

T D
$\langle \Delta R_{calc} \rangle$ vs ω_T
(for $\frac{\lambda_2}{\lambda_3} \geq 1.8$)
$\frac{\sigma_B}{B_p} = 0.04 \times J$
N = 100
J=1
2
3
4
5
6
7
8
9
10
11
12
13
14
0.00
0.02
0.04
0.06
0.08
0.10
0.12
0.14
0.16
0.18
0.20
0.22
$\langle \Delta R_{calc} \rangle$
20°
30°
45°
60°
90°
120°
ω_T

Figure 9

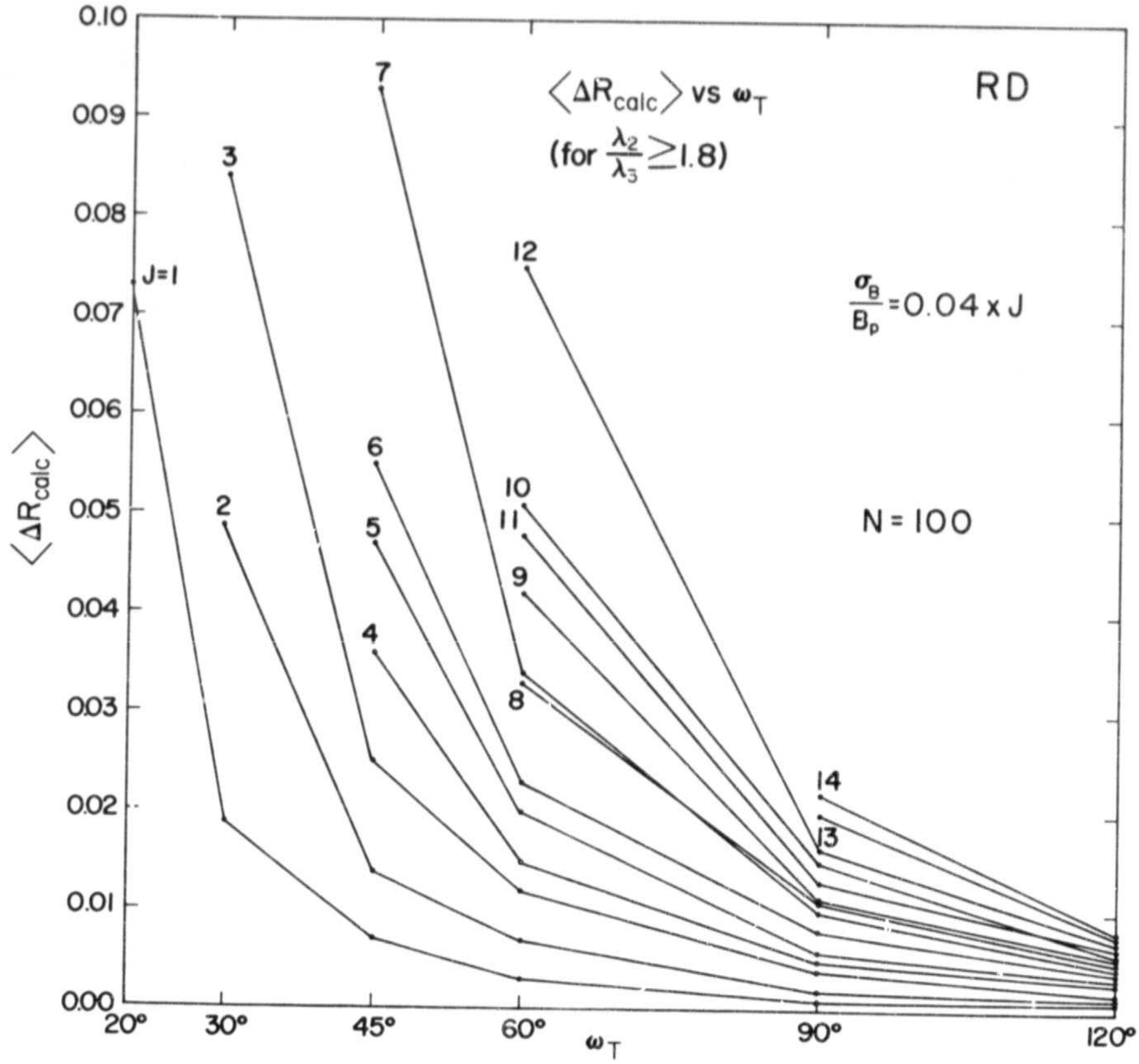

$\langle \Delta R_{calc} \rangle$ vs ω_T
(for $\frac{\lambda_2}{\lambda_3} \geq 1.8$)
RD
$\frac{\sigma_B}{B_p} = 0.04 \times J$
N = 100
$\langle \Delta R_{calc} \rangle$
ω_T
J=1
2
3
4
5
6
7
8
9
10
11
12
13
14
0.00
0.01
0.02
0.03
0.04
0.05
0.06
0.07
0.08
0.09
0.10
20°
30°
45°
60°
90°
120°

Figure 10

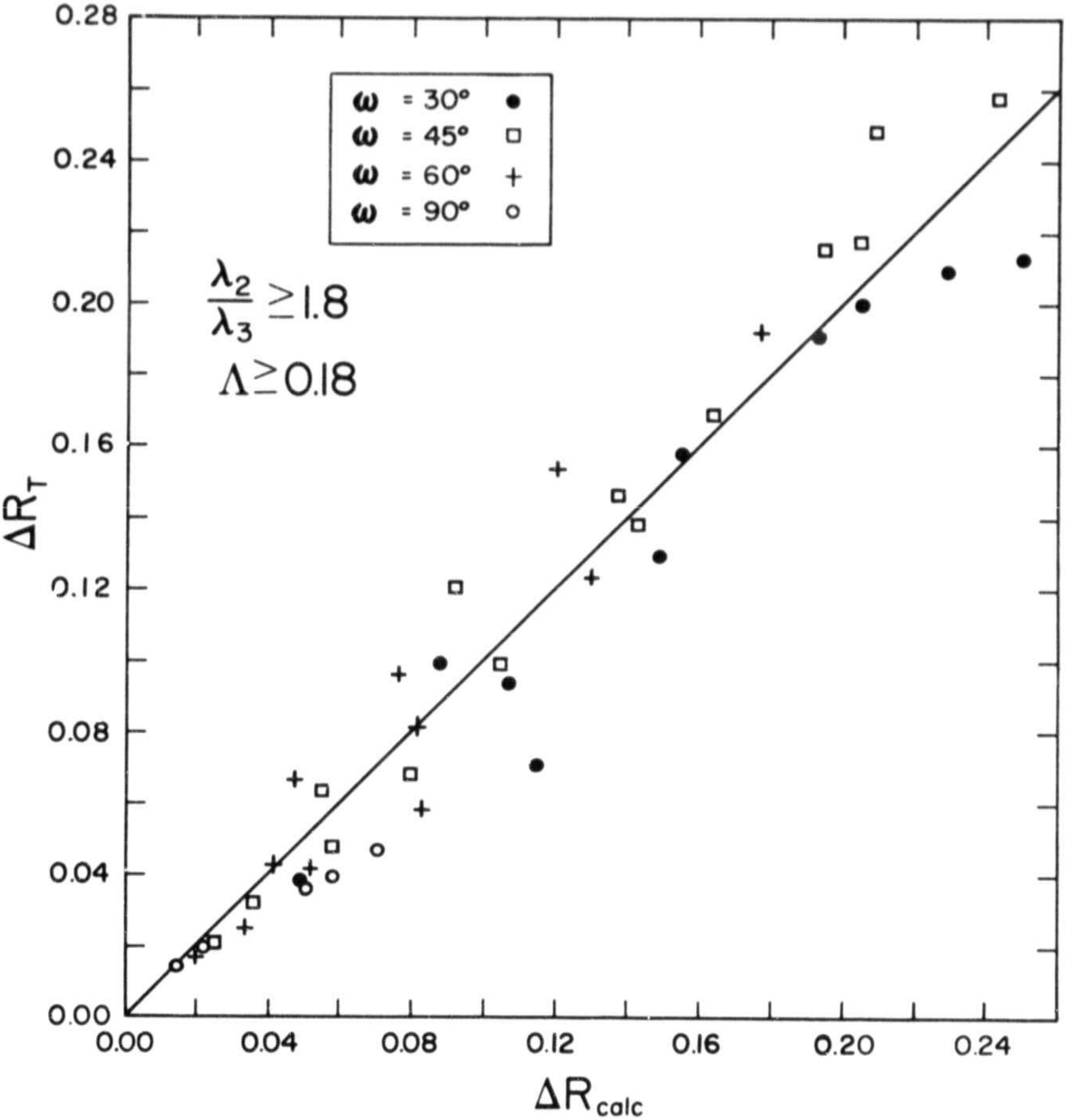
0.28
0.24
0.20
0.16
0.12
0.08
0.04
0.00
0.00
0.04
0.08
0.12
0.16
0.20
0.24
ΔR_T
ΔR_{calc}
ω = 30°
ω = 45°
ω = 60°
ω = 90°
$\frac{\lambda_2}{\lambda_3} \geq 1.8$
$\Lambda \geq 0.18$

Figure 11

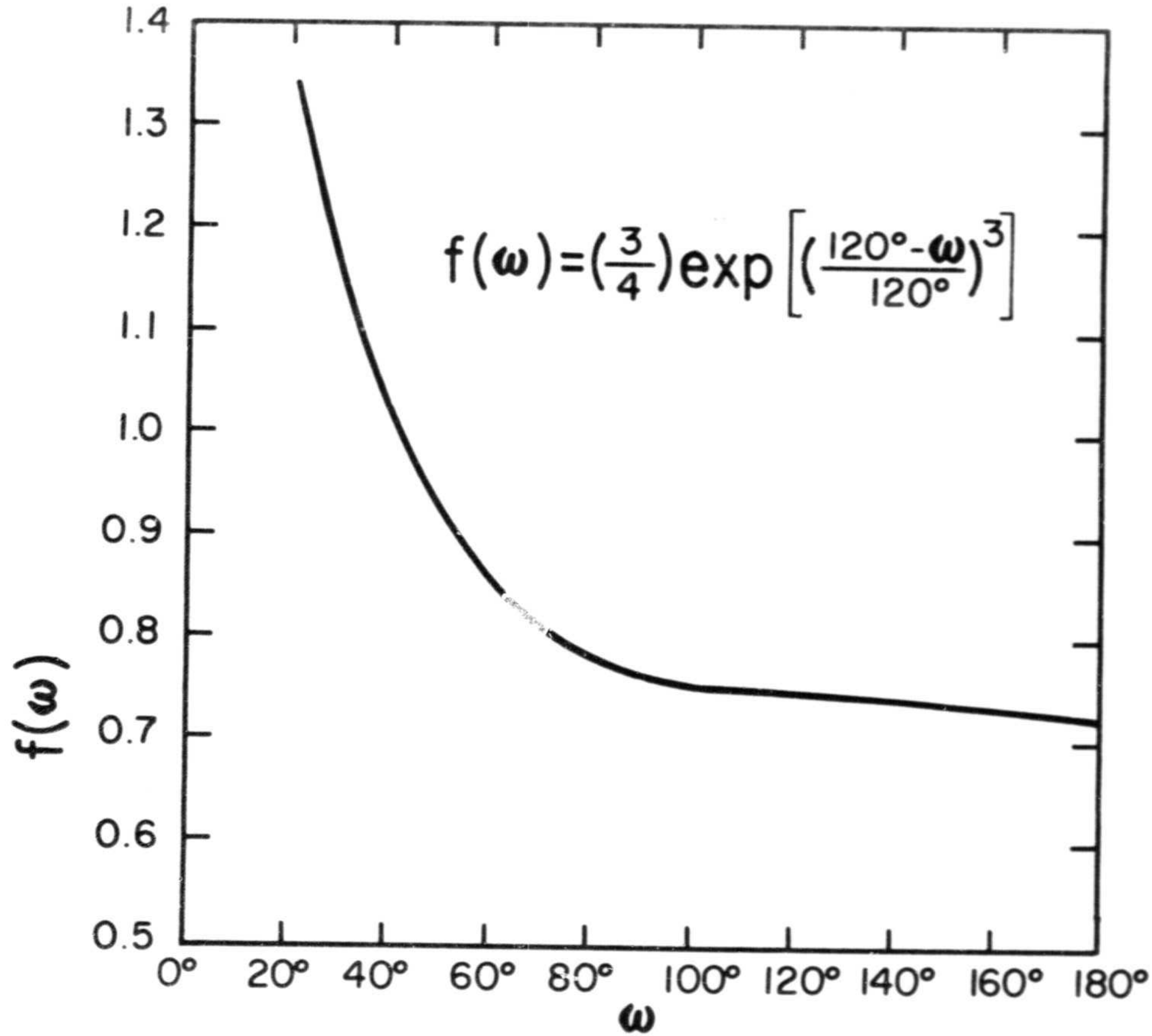

$f(\omega)=(\frac{3}{4})\exp\left[(\frac{120°-\omega}{120°})^3\right]$
1.4
1.3
1.2
1.1
1.0
0.9
0.8
0.7
0.6
0.5
f(ω)
0° 20° 40° 60° 80° 100° 120° 140° 160° 180°
ω

Figure 12

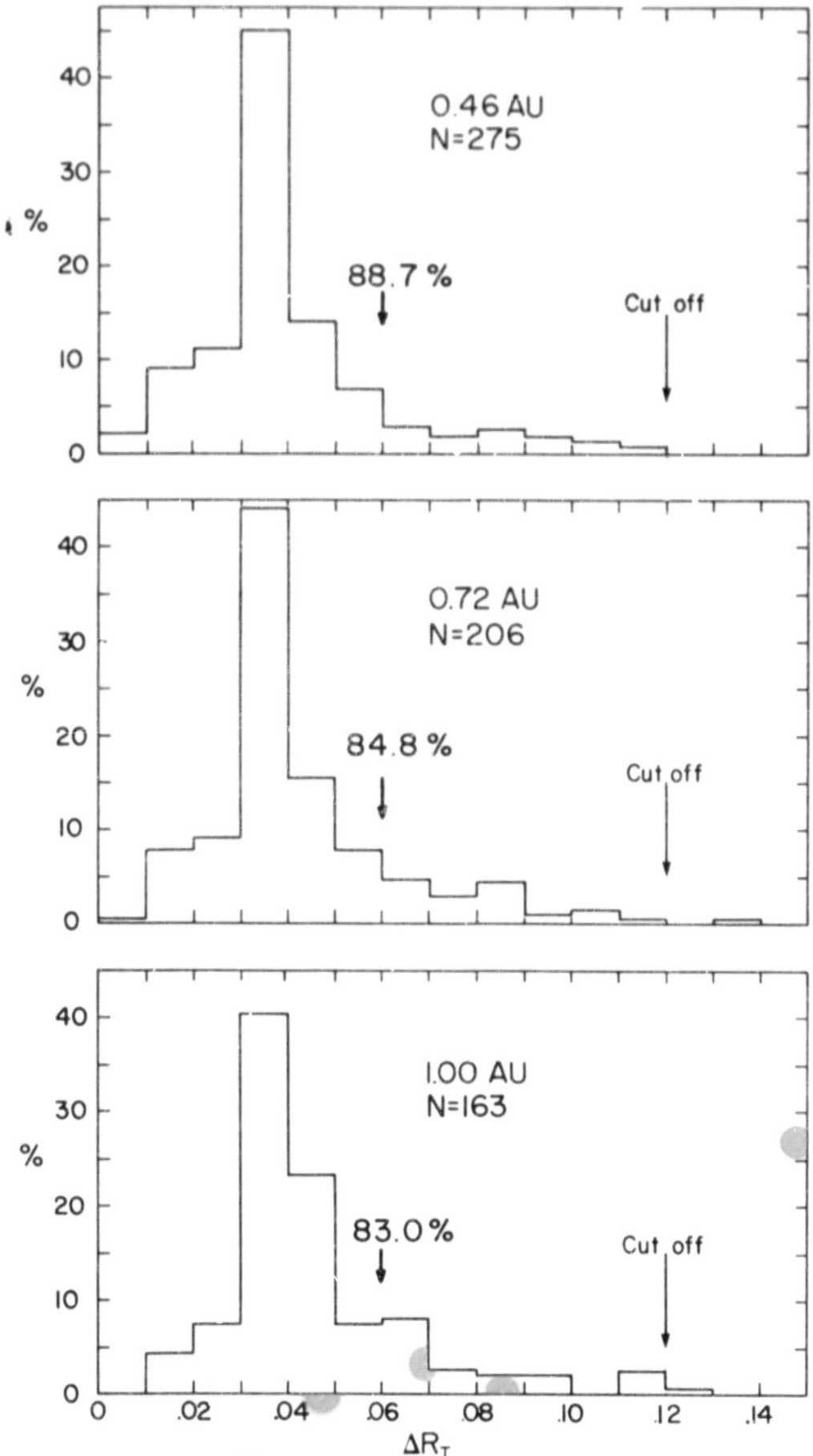
0.46 AU
N=275
88.7 %
Cut off
0.72 AU
N=206
84.8 %
Cut off
1.00 AU
N=163
83.0 %
Cut off
%
0
10
20
30
40
0
.02
.04
.06
.08
.10
.12
.14
ΔR_T

Figure 13

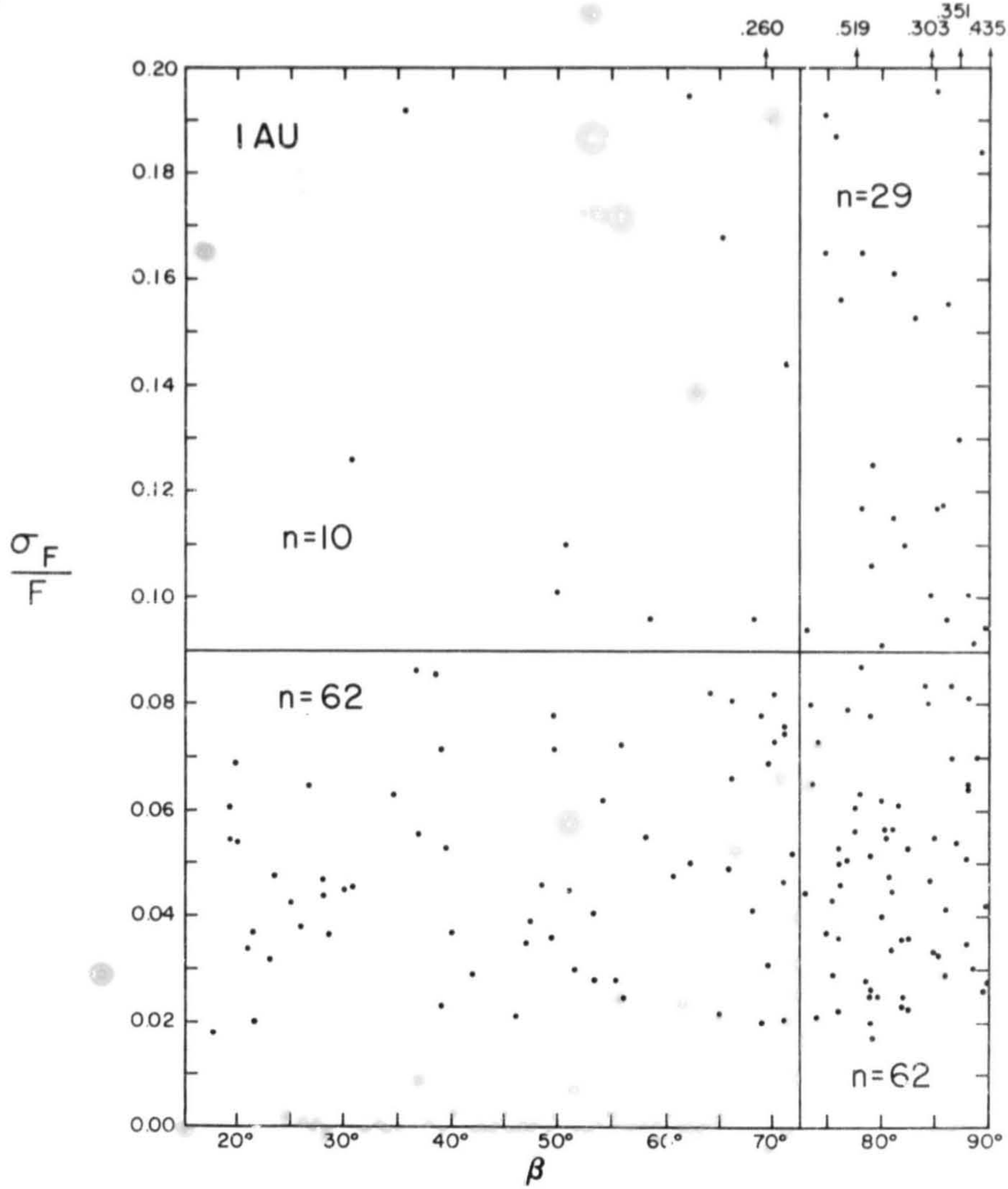

.260
.519
.303
.351
.435
1 AU
n=29
n=10
n=62
n=62
0.20
0.18
0.16
0.14
0.12
0.10
0.08
0.06
0.04
0.02
0.00
$\frac{\sigma_F}{F}$
20°
30°
40°
50°
60°
70°
80°
90°
β

Figure 14